Cytometry Part A 65A:116–123 (2005)

Alkaline Hemolysis Fragility Is Dependent on Cell Shape: Results From a Morphology Tracker

Cristian Ionescu-Zanetti,[1,2,3] Lee-Ping Wang,[1,2,3] Dino Di Carlo,[1,2,3] Paul Hung,[1,2,3] Andrea Di Blas,[4] Richard Hughey,[4] and Luke P. Lee[1,2,3]*

[1]Bioengineering Department, University of California at Berkeley, Berkeley, California
[2]Biomolecular Nanotechnology Center, University of California at Berkeley, Berkeley, California
[3]Berkeley Sensor and Actuator Center, University of California at Berkeley, Berkeley, California
[4]Computer Engineering Department, University of California at Santa Cruz, Santa Cruz, California

Received 3 November 2004; Revision Received 19 January 2005; Accepted 19 January 2005

Background: The morphometric analysis of red blood cells (RBCs) is an important area of study and has been performed previously for fixed samples. We present a novel method for the analysis of morphologic changes of live erythrocytes as a function of time. We use this method to extract information on alkaline hemolysis fragility. Many other toxins lyse cells by membrane poration, which has been studied by averaging over cell populations. However, no quantitative data are available for changes in the morphology of individual cells during membrane poration-driven hemolysis or for the relation between cell shape and fragility.

Methods: Hydroxide, a porating agent, was generated in a microfluidic enclosure containing RBCs in suspension. Automatic cell recognition, tracking, and morphometric measurements were done by using a custom image analysis program. Cell area and circular shape factor (CSF) were measured over time for individual cells. Implementations were developed in MATLAB and on Kestrel, a parallel computer that affords higher speed that approaches real-time processing.

Results: The average CSF went through a first period of fast increase, corresponding to the conversion of discocytes to spherocytes under internal osmotic pressure, followed by another period of slow increase until the fast lysis event. For individual cells, the initial CSF was shown to be inversely correlated to cell lifetime (linear regression factor R = 0.44), with discocytes surviving longer than spherocytes. The inflated cell surface area to volume ratio was also inversely correlated to lifetime (R = 0.43) but not correlated to the CSF. Lifetime correlated best to the ratio of cell inflation volume ($V_{final} - V_{initial}$) to surface area (R = 0.65).

Conclusions: RBCs inflate at a rate proportional to their surface area, in agreement with a constant flux model, and lyse after attaining a spherical morphology. Spherical RBCs display increased alkaline hemolysis fragility (shorter lifetimes), providing an explanation for the increased osmotic fragility of RBCs from patients who have spherocytosis. © 2005 Wiley-Liss, Inc.

Key terms: erythrocyte; red blood cell; spherocytosis; alkaline lysis; cell tracking; morphometric analysis; colloid-osmotic lysis; parallel computer acceleration

Hemolysis dynamics in the presence of porating agents is an important area of research due to the gamut of natural and synthetic toxins that affect cell death through membrane permeabilization (1). Poration-driven hemolysis is intrinsically dependent on the osmotic fragility of the red blood cells (RBCs) because membrane poration results in increased internal osmotic pressure by the colloid-osmotic mechanism, which in turn leads to cell lysis (2). Osmotic fragility itself has been studied extensively and is being used as a diagnostic tool for blood disorders such as spherocytosis and thalassemia. It has been shown that the osmotic fragility of spherocytic RBCs is higher than that of normal-shaped RBCs (3). However, spherocytic RBCs have a cytoskeletal protein makeup different from that of normal RBCs (4,5), a factor that could influence osmotic fragility independent of cell shape effects. It is therefore important to determine the relation between cell shape and alkaline hemolysis fragility (and osmotic fragility) for healthy RBCs. We addressed this question by measuring shape changes for individual RBCs during alkaline hemolysis.

It is generally accepted that RBCs swell before bursting after the application of membrane-porating agents (2,6). However, observations to date result from qualitative classification of fixed cells imaged by scanning electron microscopy (7), population averages obtained from forward angle scattering (8), or dielectric measurements (9).

*Correspondence to: Dr. Luke P. Lee, Department of Bioengineering, University of California at Berkeley, Berkeley, CA 94720.
E-mail: lplee@berkeley.edu
Published online 22 April 2005 in Wiley InterScience (www.interscience.wiley.com).
DOI: 10.1002/cyto.a.20135

Our aim was to directly observe a large number of single RBCs in suspension and measure morphologic changes leading to lysis. Hydroxide was used as the membrane-porating agent and applied to the cells inside a microfluidic device. Recently, we published results on the use of this device for lysis of ex vivo RBCs and cell lines (HeLa and Chinese hamster ovary) undergoing colloid-osmotic lysis (10). This previous work did not require automated cell recognition and tracking or detailed morphometric analysis. Although automated measurements of RBC morphologic parameters have been developed previously for diagnostic purposes (11–13), we extended this methodology to live cell tracking across video frames.

We present direct measurements of single cell morphology over the time (t = 10 s) before the fast lysis event (t = 60 ms) from microscopic data collected simultaneously for a large number of cells. Data analysis was done with an automated image analysis program that performed cell recognition and tracking across video frames in addition to measurements of morphologic parameters. The program was entirely custom designed and tailored to this specific application, with an extension that employs the University of California of Santa Cruz (UCSC) Kestrel parallel computer to decrease the computation time to a level approaching real-time performance.

MATERIALS AND METHODS

Microdevice Fabrication and Lytic Agent Generation

A microfluidic device (Fig. 1) was designed and fabricated for local generation of hydroxide (the lytic agent). The device design and fabrication have been described in detail elsewhere (10) and was briefly as follows. Electrodes (150-nm palladium layer on top of a 10-nm titanium adhesion layer) were photolithographically defined onto a glass slide by e-beam evaporation, followed by photoresist lift-off in acetone. Palladium was chosen as an electrode material because of its ability to electrolyze water at low voltages. The mold for the microfluidic channels and lysing chamber was fabricated by using negative photoresist (SU-8 25, Microchem Corporation; 40 μm thick). PDMS (Sylgard 184, Dow Corning Corporation) was poured on the mold and cured in a 70°C oven for 6 h. The PDMS was then carefully peeled off the mold. The fluid inlet and outlet were punched by a flat-tip needle for tube connections. The glass slide with Ti/Pd electrodes and the Polydimethylsiloxane (PDMS; Sylgard 184, Dow Corning Corp.) structures were oxygen plasma bonded.

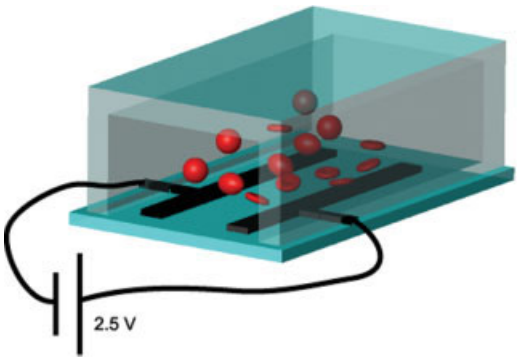

FIG. 1. Device design for local hydroxide generation. A voltage bias is applied to palladium electrodes inside a microfluidic chamber, which delivers hydroxide ions to RBCs in suspension in the vicinity of the cathode. The microfluidic chamber consists of a PDMS channel that is bonded to a glass slide containing microfabricated electrodes. Changes in cell morphology are recorded by microscopic observation of cells undergoing lysis in the vicinity of the cathode. [Color figure can be viewed in the online issue, which is available at www.interscience.wiley.com.]

The distance between electrodes was 600 μm, resulting in a field strength of 43 V/cm, an order of magnitude below minimum fields needed for electroporation-based lysis, with reported ranges of 0.3 kV/cm) (14) to 0.9 kV/cm (15). The chamber width and length were 1.5 mm × 5 mm. Chamber height was 40 μm.

After introducing a suspension of RBCs into the chamber, a constant current was applied to the electrodes (15 μA). This ensured a constant production of hydroxide at the cathode, leading to cell membrane poration and colloid-osmotic lysis of RBCs. Erythrocyte solutions were obtained by diluting defibrinated sheep blood (HemoStat Labs, Dixon, CA, USA) with phosphate buffered saline to a final hematocrit of 3.

Automated Cell Tracking and Morphometric Analysis

Image analysis was employed to recognize and track cells across multiple video frames and simultaneously measure morphologic parameters. We first developed a MATLAB (Mathworks) program to facilitate working with images (as matrices). We performed a convolution on each pixel in the image by using a hand-picked representative cell sample as the kernel (inset, Fig. 2A). Pixels with high output values from the convolution were identified as positions of cells and were labeled with solid circles on the original image (Fig. 2A). The number of cells in the image as a function of time is shown in Figure 2B.

We implemented an algorithm that tracks cells across multiple frames. Because each cell moves by only a small amount in the time interval between consecutive frames, two cells in two frames with a sufficiently small variation in distance (d < 1 μm) were identified as the same cell. This enabled us to automatically track cells and measure morphologic parameters over time. Cells that left the image and cells that entered the image after the start of the sequence were not counted.

Once the coordinates of each cell were found, we used intensity thresholding to find the cell edge: The cell center always appears bright, surrounded by a dark ring. We used intensity thresholding to find the border between the bright central region and the outer dark ring and defined this contour as the cell perimeter. The edge pixels were then fit with a smoothing spline to yield a function of radius versus central angle, $R(\theta)$. This function (cell contours, Fig. 2A) was numerically integrated to calculate the cell perimeter and area. It should be noted that this algorithm is critical to obtain accurate morphometric data that are not as affected by pixilation.

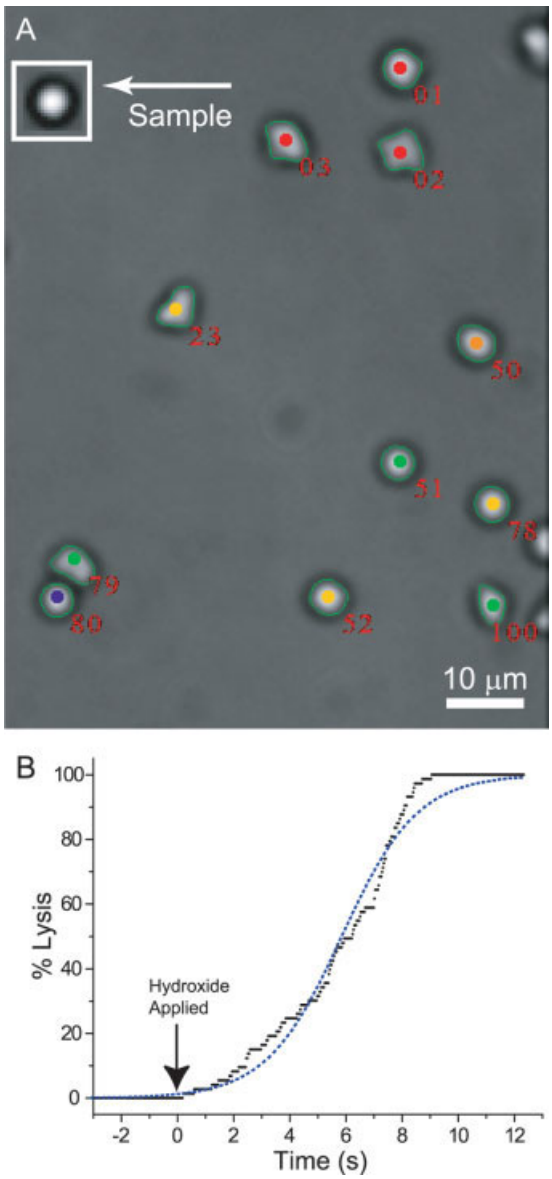

FIG. 2. Cell recognition and percentage of lysis over time. **A:** A typical frame after cell recognition and edge detection. Cells are marked by colored spots and labeled by identification numbers. The sample cell used for convoluting the image is shown in the upper left corner. The color of the spots corresponds to the quality of the match, ranging from red (90–100% of maximum convolution output) to blue (50–60% of maximum). Cell edges were found by intensity thresholding and labeled with a green contour. **B:** Percentage of lysis as a function of time for a cell lysis movie (dotted line). A gaussian distribution of lysis events corresponds well to the sigmoidal shape of the survival curve (solid line). [Color figure can be viewed in the online issue, which is available at www.interscience.wiley.com.]

To quantify cell sphericity based on the horizontal projection of each cell, we used the circular shape factor (CSF) (13), defined by:

$$\mathrm{CSF} = \frac{P_{cell}^{\ 2}}{4\pi A_{cell}}$$

Perfectly circular cells will have a CSF of 1, whereas noncircular cells will have a CSF smaller than 1. Parameters including cell position, perimeter, area, and CSF were stored in a data table for easy retrieval, data analysis, and plotting.

Computational Efficiency

The MATLAB programming environment stores variables as matrices, making it an ideal language for image processing applications. Once images are stored as matrices, thresholding and convolution operations are easily performed. However, MATLAB is an interpreted language, meaning that runtimes are much higher than for those of a similar compiled program.

We developed three implementations of our automated cell analysis program: a MATLAB implementation, a C implementation, and an enhancement of the C implementation that uses the UCSC Kestrel parallel processor to speed up parts of the computation. All implementations follow the same series of computational steps on a sequence of frames, even though the low-level details are not identical (Fig. 3A–D). The processing of each frame begins with a two-dimensional convolution, after which cells positions are identified and cells are counted. In addition, we use a simple proximity matcher to track cells across frames.

The computational times of the different implementations are reported for the processing of one frame (Fig. 3F). We single out the time required for the bidimensional convolution because its high computational load and its regular structure motivate its implementation on a parallel architecture (the Kestrel parallel computer). The Kestrel parallel processor is a Single Instruction-Multiple Data parallel computer that is entirely designed and built at the University of California at Santa Cruz and was originally targeted at computational biology applications (16,17). Kestrel is on a single PCI board for a Linux or a Windows NT host (Fig. 3E).

The bidimensional convolution is a computational step of the order of $O(N^2k^2)$ for a frame of $N \times N$ pixels and a convolution kernel of $k \times k$ pixels. The speedup we obtain performing the convolution on Kestrel is only 40% because the Kestrel prototype has a limited bandwidth over the PCI bus that penalizes I/O-bound applications. However, our goal was to evaluate the speedup that could be achieved with the new Kestrel-2 parallel processor that is being built. Kestrel-2 is based on the same architecture and technology as Kestrel but has twice as many processing elements, runs at twice the clock speed, and has a much improved I/O bandwidth. For Kestrel-2 the convolution will take less than 20% of the total computation time. Implementing additional computational steps on Kestrel-2 or simply using a more powerful serial machine as the front end will further improve the performance. The data in the table (Fig. 3F) show that the Kestrel-2 implementation will approach real-time processing, thus enabling additional applications such as real-time sorting of cells based on morphologic parameters.

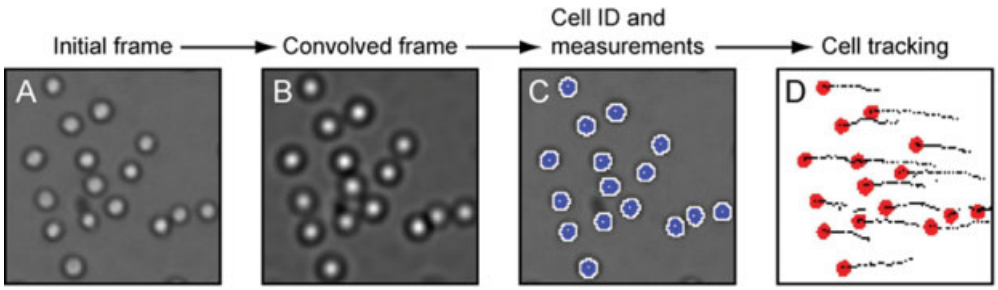

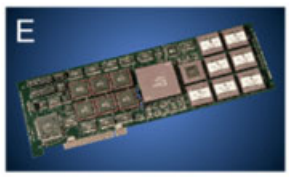

F

	Time / frame	Frames/s	Speedup
MATLAB	53 s (60% conv .)	0.02	1.0
C	0.96 s (92% conv .)	1.04	55.2
C + Kestrel	0.72 s (90% conv .)	1.38	73.6
C + Kestrel -2	87 ms (19% conv .)	11.50	609

FIG. 3. Image processing pipeline and comparative performance of our implementations. The main computational steps in our programs for a region of sample frame are **A:** image acquisition, **B:** image convolution with a cell kernel, **C:** identification of cell centers and perimeters and **D:** cell tracking across multiple frames. **E:** The UCSC Kestrel parallel computer PCI board. **F:** Computational times for 512- × 512-pixel frames with 8 bits/pixel and a convolution kernel of 15 × 15 pixels. Convolution, cell identification, and tracking were performed on a 1-GHz Pentium III and the Kestrel or Kestrel-2 (currently in its final design stage—projected performance) parallel computers. [Color figure can be viewed in the online issue, which is available at www.interscience.wiley.com.]

RESULTS

Time Course of Morphologic Transformations

Our method of hydroxide-driven lysis was presented previously (10), and it proceeds as follows. A DC bias (2.6 V) is applied to two palladium electrodes inside a microfluidic enclosure, resulting in the production of hydroxide ions at the cathode (Fig. 1). In the presence of hydroxide, RBCs first swell and then undergo fast radial expansion and lysis. Poration and swelling last 5 to 10 s and are followed by fast lysis, which occurs within 60 ms. We examined the effect of membrane poration on RBC shape before the fast lysis event. During the fast lysis event, pore size is increased quickly by osmotic pressure in a positive feedback mechanism (10).

Sequential frames were captured every 33 ms in phase contrast mode with a camera attached to an inverted microscope. Using an automated image analysis program, we were able to recognize and track cells across video frames (Fig. 3). Cells were tracked across multiple frames, enabling the monitoring of cell shape changes over time.

For each cell, the perimeter, area, and CSF were calculated as a function of time (see Materials and Methods).

The survival curve (percentage of the initial population lysed as a function of time) for a movie containing 71 cells is shown in Figure 2B. Note that hydroxide application is initiated at $t = 0$ s (Fig. 2B) and lysis of the cell sample is completed at $t = 10$ s. The average cell lifetime is 5.6 ± 2.2 s. This curve is equivalent to survival curves customarily presented in the hemolysis literature (6,18,19). The marked difference is that our survival curve is quantized, with steps representing individual lysis events. For this experiment the observed area was surrounded on three sides by OH^--generating electrodes, and there was no dependence of cell lifetime on the distance from the electrode edge (data not shown, $R = 0.03$).

Individual cells had a diverse range of behaviors. Data for area and CSF as a function of time are presented for three representative cells (Fig. 4). The large differences in cell data obtained were largely due to the discocyte orientation with respect to the microscope objective because we were presented with only two-dimensional projections of the true three-dimensional cell geometry. A side view of the discocyte shows an elliptical projection that expands (Fig. 4A). The front view projection is circular and shrinks first during the transition to a spherical morphology and is followed by an increase shortly before lysis (Fig. 4B). Rotating cells produce a time-dependent oscillation between the two regimes (Fig. 4C). If averaging over a large cell sample, we expect to obtain a mean over all possible cell orientations. To obtain a better picture of cell shape leading to the lysis event, we time-shifted all morphometric parameter plots so that every cell underwent fast lysis at the same time, $t = 4.5$ s (Fig. 5).

Cell projection area onto the horizontal plane did not increase uniformly (Fig. 5A). There was no marked change in average area for the first 2 s of hydroxide application. This result agrees with a simple qualitative prediction: A healthy discocyte appears circular from a front view but elliptical from a side view. As fluid entered the cell, the cell's volume would increase. Suppose the total membrane surface area remains constant. Then, as the erythrocyte shape approaches a sphere, the frontal view shrinks and the side view grows in size. Only immediately before the lysis event ($t > 4$ s) did we observe a uniform increase in cell area. This corresponds to the cell assuming a spherical morphology, after which

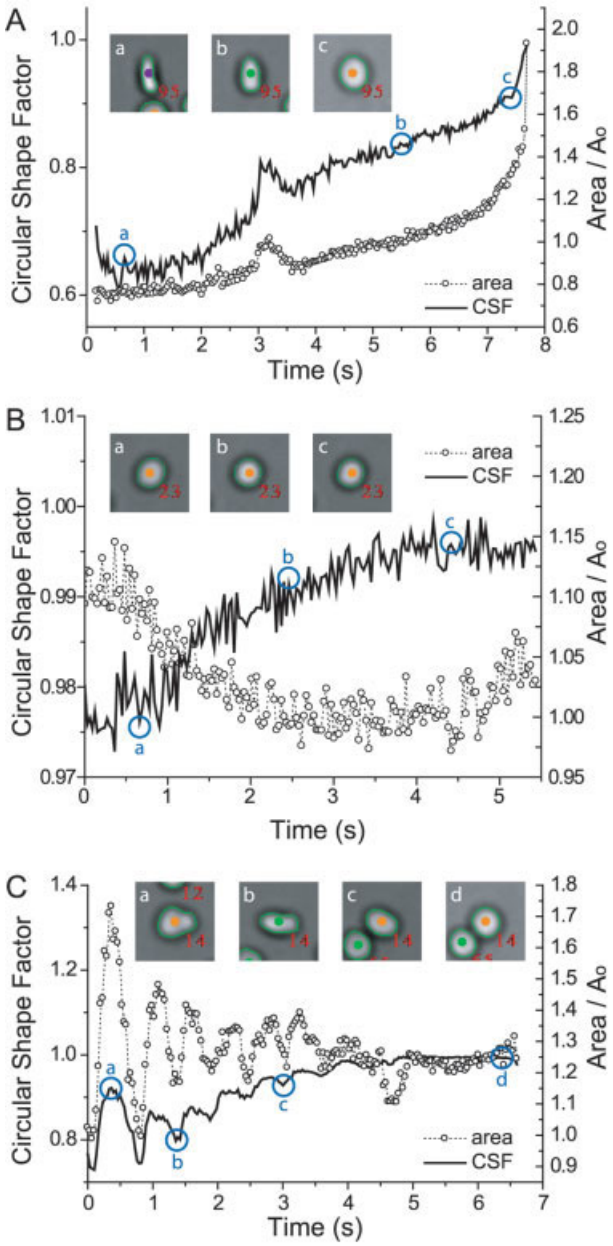

FIG. 4. Morphologic analysis of three representative cells before lysis. CSF (solid line) and cell projection area (dotted line) are plotted with respect to time (note different scales). **A:** Side view of a cell at constant orientation. Area and CSF are monotonically increasing. **B:** Frontal view of a cell at constant orientation. This cell goes through much smaller changes in size and CSF. However, its size is slightly decreasing. These results agree with a front view of a discoid shape that is slowly converted to a sphere. **C:** This cell is simultaneously flipping over and changing to a spherical shape. This results in an oscillating CSF that increases over time. It also causes an increase in size of the side projection and a decrease of the frontal projection, so that the oscillation amplitude for area measurements decreases. [Color figure can be viewed in the online issue, which is available at www.interscience.wiley.com.]

the pressure difference across the cell membrane causes the membrane to stretch, leading to our observed area increase before lysis.

Our averaged results showed that the average CSF increased uniformly as cells approached the lysis event (Fig. 5B). None of the cells examined showed a uniform decrease in CSF, although some cells remained constant. The average CSF goes through a first period of fast increase, corresponding to the conversion of discocytes and echinocytes to spherocytes due to internal osmotic pressure (t = 0–2.5 s), followed by another period of slow increase until the fast lysis event (t = 2.5–4.5 s).

Lifetime Dependence on Cell Shape

At the start of the experiment, RBCs exhibited a distribution of shapes, from discocytes to e spherocytes. We measured lifetimes for individual cells and, hence, influence of individual cell shape on alkaline hemolysis fragility.

The first morphologic parameter measured was CSF. The minimum CSF over the first 20 movie frames (0.66 s) was recorded to be representative of initial RBC shape in the side view. A linear fit to the scatter plot of lifetime ver-

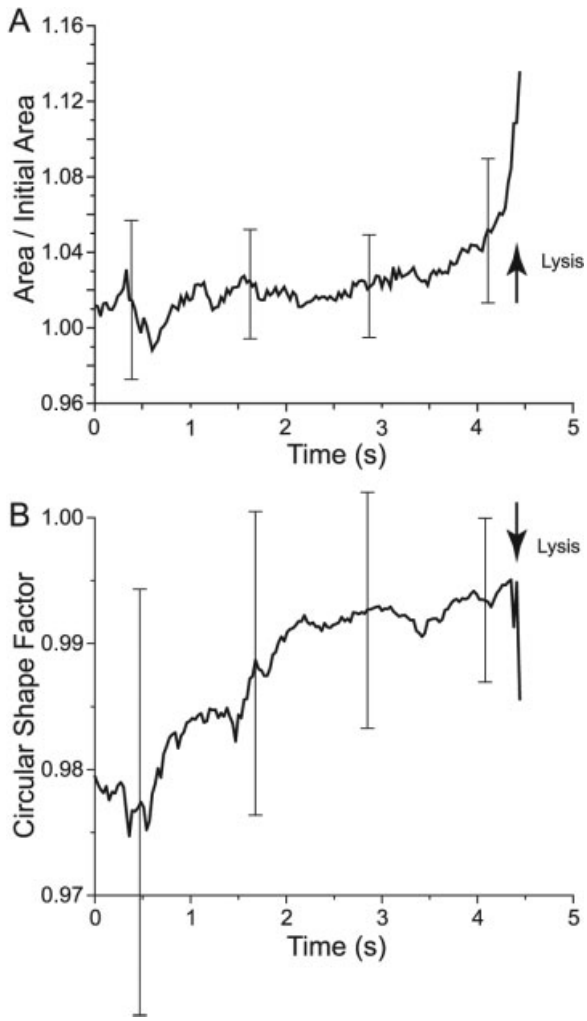

FIG. 5. Average cell area and CSF over the cell population as a function of time. **A:** Cell projection area change as a function of time. **B:** CSF change as a function of time. Time scales for each cell were normalized to a common time of lysis (4.5 s) before taking the mean. Error bars represent 0.5 standard deviation from the mean above and below the graph. The large standard deviation in the data is caused by the diversity of the cell shape and orientation across the population.

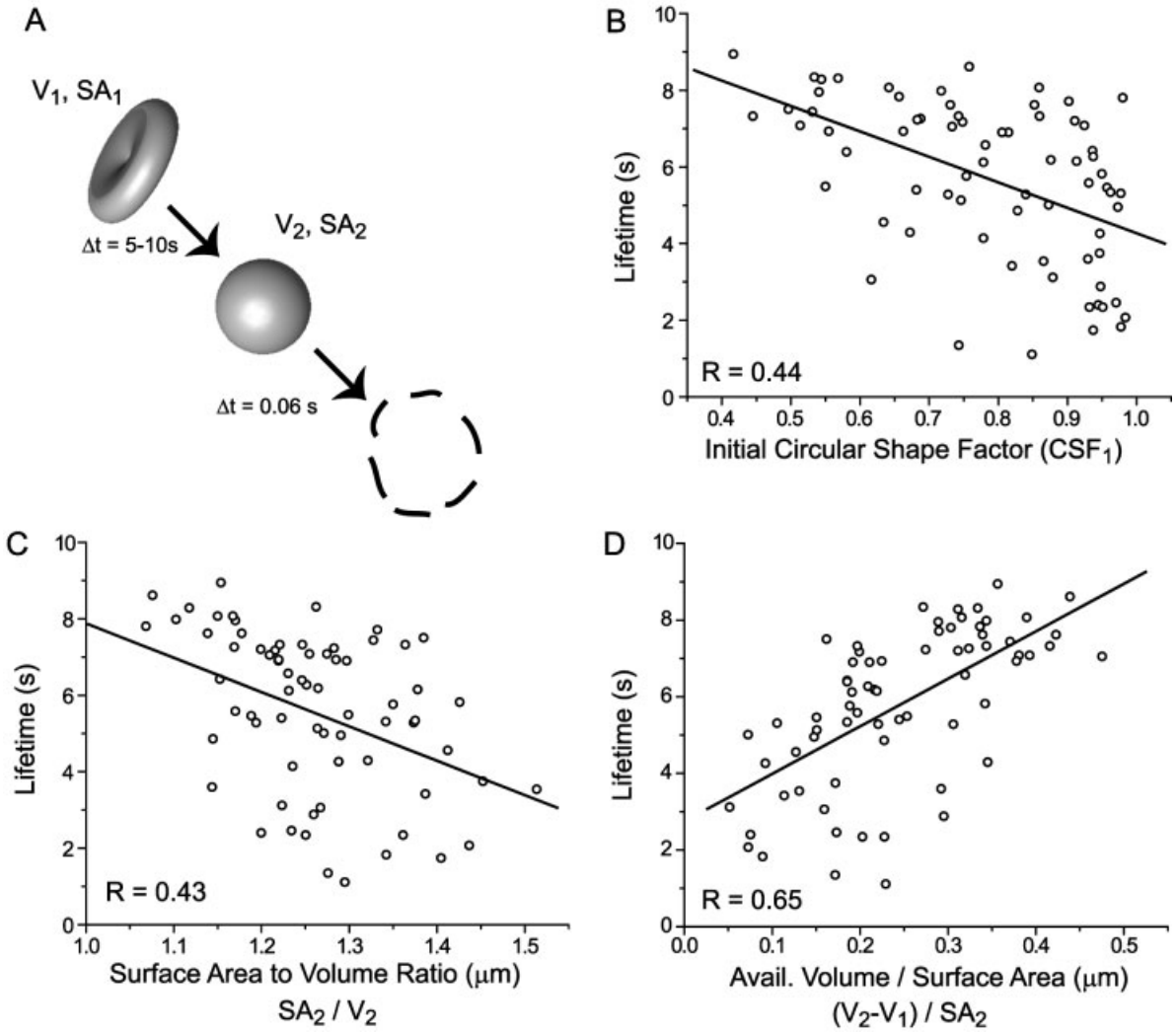

FIG. 6. Cell lifetime dependence on morphometric parameters. **A:** Cartoon representation of changes in cell shape from initial discocyte (volume V_1, surface area SA_1) to final spherical shape before lysis (V_2, SA_2). Scatter plots relate lifetime to initial CSF (**B**), final spherical SAV ratio (**C**), and the inflation volume to surface area ratio (**D**). The initial CSF was taken as the minimum over the first 20 frames (0.66 s) of cell lifetime to account for cell rotation. C: The final SAV ratio was averaged over the final 20 frames (0.66 s) before lysis. Lifetime is inversely correlated with initial CSF (R = 0.44) and final SAV ratio (R = 0.43). D: The best correlation is found between lifetime and the inflation volume to surface area ratio, in agreement with a constant flux per unit area model.

sus initial CSF shows the two to be inversely correlated (R = 0.44, Fig. 6B).

Another important parameter is the ratio of surface area to volume (SAV) for the inflated cell. For an RBC that has reached the spherical stage, the SAV is given by:

$$\frac{A_{surface}}{V_{final}} = \frac{4\pi R^2}{\frac{4}{3}\pi R^3} = \frac{3}{R}$$

Because poration is a surface phenomenon, we expect lifetime to be inversely correlated to the SAV ratio in the spherical stage (before the fast lysis event). Figure 6C shows that the two are indeed inversely correlated (R = 0.43), about as strongly as lifetime and initial CSF (R = 0.44). An important internal check is to verify that initial CSF does not correlate with spherical SAV. The data show no correlation, with a linear regression coefficient of R = 0.01 (data not shown). In Figure 6D, we plot lifetime as a function of the inflation volume over cell surface area, $(V_{final} - V_{initial})/A_{surface}$. This measurement shows the best correlation to cell lifetime (R = 0.65).

DISCUSSION

Hydroxide reacts with cell membranes by cleaving constituent molecules into fatty acids and lysophospholipids, a process known as saponification (20). As the nomenclature suggests, lysophospholipids have been shown to porate cell membranes and lead to lysis when added to extracellular media (21). Therefore, hydroxide application is likely to lead to lysophospholipid-mediated poration of the cell membrane. The pores allow small ions to permeate the membrane and keep larger anionic proteins in the cytoplasm. Small ions and associated water molecules enter the cell, creating a positive osmo-

tic pressure. The swelling and subsequent bursting of the cell, referred to as colloid-osmotic lysis (6), was shown to be a conserved mechanism for a large number of pore-forming compounds, from bacterial toxins to viral capsids (1).

We measured morphologic parameters for single cells undergoing this process with two aims in mind: (a) to quantify morphologic changes before fast lysis and (b) to determine the influence of initial cell shape on alkaline hemolysis fragility. Automated analysis of RBC morphology from single images has been reported previously, with an emphasis on the diagnosis of sickle cell anemia (11,12,22). These measurements were taken on fixed cells between microscope slides, whereas we measured the morphology of live cells in a microfluidic enclosure. In addition to developing our own method for measuring morphometric parameters, we implemented cell tracking across multiple frames, enabling the monitoring of cell shape changes ex vivo over time. The analysis of program runtimes suggests that real-time processing of the image data will be possible by using a parallel accelerator, such as the UCSC Kestrel parallel computer (see Materials and Methods; Fig. 3).

Morphometric parameters were averaged over the cell population after offsetting the time scale such that all cells underwent fast lysis simultaneously, at t = 4.5 s. The average CSF (sphericity) goes through a period of fast increase (t = 0–2.5s), after which it remains constant until the lysis event (t = 2.5–4.5s). This result suggests a relation between the pressure required to overcome the RBC shape-conserving factors and the pressure required to overcome the membrane tensile strength. An exact relation would require knowledge of the rate of increase in internal osmotic pressure as a function of time, in addition to the present data on cell shape. If we make the simple assumption that pressure increases at a constant rate, morphometric data show that shape-conserving factors are overcome by about half the pressure required to overcome membrane tensile strength (Fig. 5B). Erythrocyte shape is believed to be governed by a combination of bilayer coupling and the membrane-associated cytoskeleton (23). In the future, measurements of cell morphologic changes in the presence of cytoskeleton-disruptive agents or membrane-coupling alteration compounds can be used to discriminate between the two shape-control mechanisms.

The second parameter measured was cell area, or rather the cell's projection onto the horizontal plane. As described above, for the first half of the cell's lifetime, discocytes convert to spherocytes due to increased internal osmotic pressure and swelling. This process can lead to increases or decreases of cell area, depending on the discocyte orientation with respect to the horizontal optical plane. This result is illustrated well by the sample cell shown in Figure 3C: because the cell is rotating, the peaks in the area graph correspond to a frontal view, whereas troughs occur for side views. During the transition to a sphere (t = 0–5 s), the side view area increases and the frontal view area decreases, but the average area remains approximately constant until the last second (t = 6–7 s), when there is a monotonic increase. One could simulate the predicted change in projection area shape and size as a function of flux with the assumption of a constant surface area for the cell. However, without determining the discocyte orientation, the model predictions would be impossible to check. The uncertainty in the cell orientation constitutes the most serious impediment to extracting the three-dimensional cell shape from our two-dimensional data. However, because the orientation angle is likely to be random, averages over a large number of individual cells will exhibit the correct behavior.

The influence of individual cell shape on alkaline hemolysis fragility can be elucidated by correlating cell lifetimes to morphologic parameters. At the start of the experiment, RBCs exhibited a continuous distribution of shapes, from discocytes and echinocytes to spherocytes. Our data show that sphericity (CSF) is inversely correlated to cell lifetime (Fig. 6B, R = 0.44). This relation is present despite the measurement noise introduced by the distribution in RBC orientation. Orientation may make some discocytes appear spherical. Therefore, a larger scatter in lifetimes is observed for cells that appear spherical (CSF > 0.96).

Alkaline lysis fragility is dependent on osmotic fragility. Therefore, this relation is consistent with a constant flux model for colloid-osmotic lysis: Discocytes start out with a smaller SAV ratio; therefore, for a constant inward flux per membrane area, the transition to spherocytes causes a delay in the application of osmotic pressure to the taut spherocyte membrane. This relation agrees well with data showing that spherocytotic RBCs have a greater osmotic fragility (3). In spherocytosis, a patient's RBCs assume a spherical shape due to defects in RBC membrane-associated cytoskeletal proteins (4,5). However, osmotic fragility measurements on spherocytotic cells leave open the possibility that osmotic fragility is not due to cell shape alone, but to differences between the cytoskeletal makeup of spherocytotic and normal RBCs. In this context, our data show that normal RBCs that are spherical also display a greater osmotic fragility. This is an important result, showing that morphology alone can be responsible for increased osmotic fragility.

Membrane poration is a surface phenomenon, whereas osmotic pressure buildup due to flux across the membrane is dependent on the fractional increase in total cell volume. Thus cell lifetimes should depend on the SAV ratio, which is dependant on the initial cell shape (as described above) and the total cell size in the spherical stage. Spherical cell size was determined by measuring the cell projection area in the final stages before lysis, when there is no dependence on cell orientation. The spherical cell radius is inversely correlated to the final SAV ratio (defined as SA_2/V_2 in Fig. 6A). The final SAV ratio is inversely correlated to lifetimes but no correlated to the initial CSF (Fig. 6C, R = 0.43). If we assume a constant flux per unit area into the cell, lifetime should change with the ratio between the inflation volume and the surface area at the spherical stage. The total inflation volume over the duration of the experiment can be calculated by

subtracting the initial volume (V_1, in the discocyte state) from the final volume (V_2, in the spherocyte state). Figure 6D shows that the best correlation to cell lifetimes is found by looking at the inflation SAV ratio, a metric that includes measurements on the initial cell shape and the final cell size. We therefore conclude that osmotic fragility is higher for cells that are initially more spherical or smaller than average.

In conclusion, we present data on morphologic parameter changes for RBCs in the presence of hydroxide, a membrane-porating agent. Measurements of individual cell data were performed by using image analysis tools for automated cell tracking and morphometric measurements designed and implemented in our laboratory. The most important result is the dependence of alkaline hemolysis fragility (and osmotic fragility) of individual cells on their inflation SAV ratio. This ratio is dependent on initial cell shape (discocyte vs. spherocyte) and cell size (cell radius in the spherical phase). The relation shows that a constant flux per unit area model fits the data on poration-driven lysis. This model also predicts that the higher osmotic fragility associated with the blood disorder spherocytosis, which exhibits spherical RBC shapes, may be explained by cell shape alone. The methods outlined in this report will be instrumental in future studies of RBC morphologic changes in response to physiologic toxins.

ACKNOWLEDGMENTS

The authors thank Nima Aghdam for three-dimensional graphic design. This work was supported in part by EIA-9722730 from the National Science Foundation to A.D.B. and R.H. The authors acknowledge financial support from the NSF (C.I.Z.) and the Whitaker Foundation (D.D.).

LITERATURE CITED

1. Bashford CL, Alder GM, Menestrina G, Micklem KJ, Murphy JJ, Pasternak CA. Membrane damage by hemolytic viruses, toxins, complement, and other cytotoxic agents—a common mechanism blocked by divalent-cations. J Biol Chem 1986;261:9300–9308.
2. Delano MD. Simple physical constraints in hemolysis. J Theor Biol 1995;175:517–524.
3. Pribush A, Hatskelzon L, Kapelushnik J, Meyerstein N. Osmotic swelling and hole formation in membranes of thalassemic and spherocytic erythrocytes. Blood Cells Mol Dis 2003;31:43–47.
4. Tse WT, Lux SE. Red blood cell membrane disorders. Br J Haematol 1999;104:2–13.
5. Bolton-Maggs PHB, Stevens RF, Dodd NJ, Lamont G, Tittensor P, King MJ, Haematology BCS. Guidelines for the diagnosis and management of hereditary spherocytosis. Br J Haematol 2004;126:455–474.
6. Pooler JP. The kinetics of colloid osmotic hemolysis 1. Nystatin-induced lysis. Biochim Biophys Acta 1985;812:193–198.
7. Vives MA, Infante MR, Garcia E, Selve C, Maugras M, Vinardell MP. Erythrocyte hemolysis and shape changes induced by new lysine-derivate surfactants. Chem Biol Interact 1999;118:1–18.
8. Harris RW, Sims PJ, Tweten RK. Evidence that *Clostridium perfringens* theta-toxin induces colloid-osmotic lysis of erythrocytes. Infect Immun 1991;59:2499–2501.
9. Pribush A, Meyerstein D, Meyerstein N. Kinetics of erythrocyte swelling and membrane hole formation in hypotonic media. Biochim Biophys Acta Biomembr 2002;1558:119–132.
10. Di Carlo D, Ionescu-Zanetti C, Zhang Y, Hung P, Lee LP. On-chip cell lysis by local hydroxide generation. *Lab on a Chip* 2005:171–178.
11. Bacus JW. Cytometric approaches to red blood cells. Pure Appl Chem 1985;57:593–598.
12. Horiuchi K, Ohata J, Hirano Y, Asakura T. Morphologic studies of sickle erythrocytes by image analysis. J Lab Clin Med 1990;115:613–620.
13. Robinson RD, Benjamin LJ, Cosgriff JM, Cox C, Lapets OP, Rowley PT, Yatco E, Wheeless LL. Textural differences between Aa and Ss blood specimens as detected by image analysis. Cytometry 1994;17:167–172.
14. Gao J, Yin XF, Fang ZL. Integration of single cell injection, cell lysis, separation and detection of intracellular constituents on a microfluidic chip. Lab on a Chip 2004;4:47–52.
15. McClain MA, Culbertson CT, Jacobson SC, Allbritton NL, Sims CE, Ramsey JM. Microfluidic devices for the high-throughput chemical analysis of cells. Anal Chem 2003;75:5646–5655.
16. Di Blas A, Dahle DM, Diekhans M, Grate L, Hirschberg J, Karplus K, Keller H, Kendrick M, Mesa-Martinez FJ, Pease D, et al. The UCSC Kestrel parallel processor. IEEE Trans Parallel Distrib Syst 2005;16:80–92.
17. Hirschberg JD, Dahle DM, Karplus K, Speck D, Hughey R. Kestrel: A programmable array for sequence analysis. J VLSI Signal Process 1998;19:115–126.
18. Shalel S, Streichman S, Marmur A. Modeling surfactant-induced hemolysis by Weibull survival analysis. Colloids Surfaces B Biointerf 2003;27:223–229.
19. Shalel S, Streichman S, Marmur A. The use of hemolysis kinetics to evaluate erythrocyte-bound surfactant. Colloids Surfaces B Biointerf 2003;27:215–222.
20. Voet D, Voet JG, Pratt CW. Fundamentals of biochemistry. New York: John Wiley & Sons; 1999. p 223–226.
21. Bierbaum TJ, Bouma SR, Huestis WH. Mechanism of erythrocyte lysis by lysophosphatidylcholine. Biochim Biophys Acta 1979;555:102–110.
22. Wheeless LL, Robinson RD, Lapets OP, Cox C, Rubio A, Weintraub M, Benjamin LJ. Classification of red blood cells as normal, sickle, or other abnormal, using a single image-analysis feature. Cytometry 1994;17:159–166.
23. Nakao M. New insights into regulation of erythrocyte shape. Curr Opin Hematol 2002;9:127–132.